JOURNAL OF GEOPHYSICAL RESEARCH, VOL. 112, F02025, doi:10.1029/2006JF000644, 2007

Characterizing arid region alluvial fan surface roughness with airborne laser swath mapping digital topographic data

Kurt L. Frankel[1] and James F. Dolan[1]

Received 25 July 2006; revised 14 November 2006; accepted 5 January 2007; published 26 May 2007.

[1] Range-front alluvial fan deposition in arid environments is episodic and results in multiple fan surfaces and ages. These distinct landforms are often defined by descriptions of their surface morphology, desert varnish accumulation, clast rubification, desert pavement formation, soil development, and stratigraphy. Although quantifying surface roughness differences between alluvial fan units has proven to be difficult in the past, high-resolution airborne laser swath mapping (ALSM) digital topographic data are now providing researchers with an opportunity to study topography in unprecedented detail. Here we use ALSM data to calculate surface roughness on two alluvial fans in northern Death Valley, California. We define surface roughness as the standard deviation of slope in a 5-m by 5-m moving window. Comparison of surface roughness values between mapped fan surfaces shows that each unit is statistically unique at the 99% confidence level. Furthermore, there is an obvious smoothing trend from the presently active channel to a deposit with cosmogenic ^{10}Be and ^{36}Cl surface exposure ages of ~70 ka. Beyond 70 ka, alluvial landforms become progressively rougher with age. These data suggest that alluvial fans in arid regions smooth out with time until a threshold is crossed where roughness increases at greater wavelength with age as a result of surface runoff and headward tributary incision into the oldest surfaces.

Citation: Frankel, K. L., and J. F. Dolan (2007), Characterizing arid region alluvial fan surface roughness with airborne laser swath mapping digital topographic data, *J. Geophys. Res.*, *112*, F02025, doi:10.1029/2006JF000644.

1. Introduction

[2] Alluvial fans are common features along the piedmonts of steep mountain fronts where streams exit the narrow confines of their source canyons, resulting in a reduction in stream power and a consequent decrease in the ability of the streams to carry large sediment loads [*Bull*, 1977]. In arid environments, this range-front deposition tends to be episodic, can be punctuated by erosion, and is commonly expressed as multiple generations of alluvial fan surfaces [*Bull*, 1991]. Alluvial fans are important recorders of both climatic and tectonic signals; alluvium of varying age can contain vast amounts of information about climatic influences on deposition, or lack thereof, as well as rates and styles of tectonism and as such, have been studied extensively [*Gilbert*, 1877; *Davis*, 1905; *Blackwelder*, 1931; *Denny*, 1967; *Bull*, 1977; *Wallace*, 1977; *Bull*, 1984; *Wells et al.*, 1987; *Lubetkin and Clark*, 1988; *Bull*, 1991; *Whipple and Dunne*, 1992; *Ritter et al.*, 1993; *Bierman et al.*, 1995; *Matmon et al.*, 2005; *Nichols et al.*, 2006; *Bull*, 2007].

[3] Discrete alluvial units are often defined by descriptions of surface morphology, desert varnish accumulation, clast rubification, desert pavement formation, soil development, and stratigraphic relationships [*Wells et al.*, 1987; *Bull*, 1991; *Ritter et al.*, 1993]. In particular, studies of soil development on desert piedmonts have been especially useful in deciphering ages of alluvial landforms and rates of fan deposition [*Birkeland*, 1999]. Recent advances in Quaternary geochronology are allowing researchers to further quantify rates of arid-region geomorphic processes [e.g., *Nichols et al.*, 2002, 2005, 2006; *Matmon et al.*, 2006].

[4] In general, alluvial fan units are mapped on aerial photographs and topographic maps using the above criteria, in conjunction with elevation above active channels, in order to determine lithostratigraphic divisions. Quantifying the topographic characteristics and differences between multiple fan surfaces, however, has been difficult with previously available maps and remotely sensed data because they generally lack the spatial resolution necessary to make a quantitative comparison between individual alluvial fan deposits [e.g., *Farr and Chadwick*, 1996]. Field techniques, such as clast-size counts or topographic surveying, while useful, are labor-intensive and usually limited in their spatial extent, therefore providing data on only a small segment of any single alluvial unit. Recently, however, the emergence of high-resolution airborne laser swath mapping (ALSM; also known as light detection and ranging or LiDAR) technology has renewed interest in the quantitative characterization of alluvial and colluvial landforms [*McKean and Roering*, 2004; *Glenn et al.*, 2006; *Staley et al.*, 2006].

[5] ALSM digital topographic data are now providing researchers with the opportunity to study landforms in

[1]Department of Earth Sciences, University of Southern California, Los Angeles, California, USA.

0148-0227/07/2006JF000644$09.00

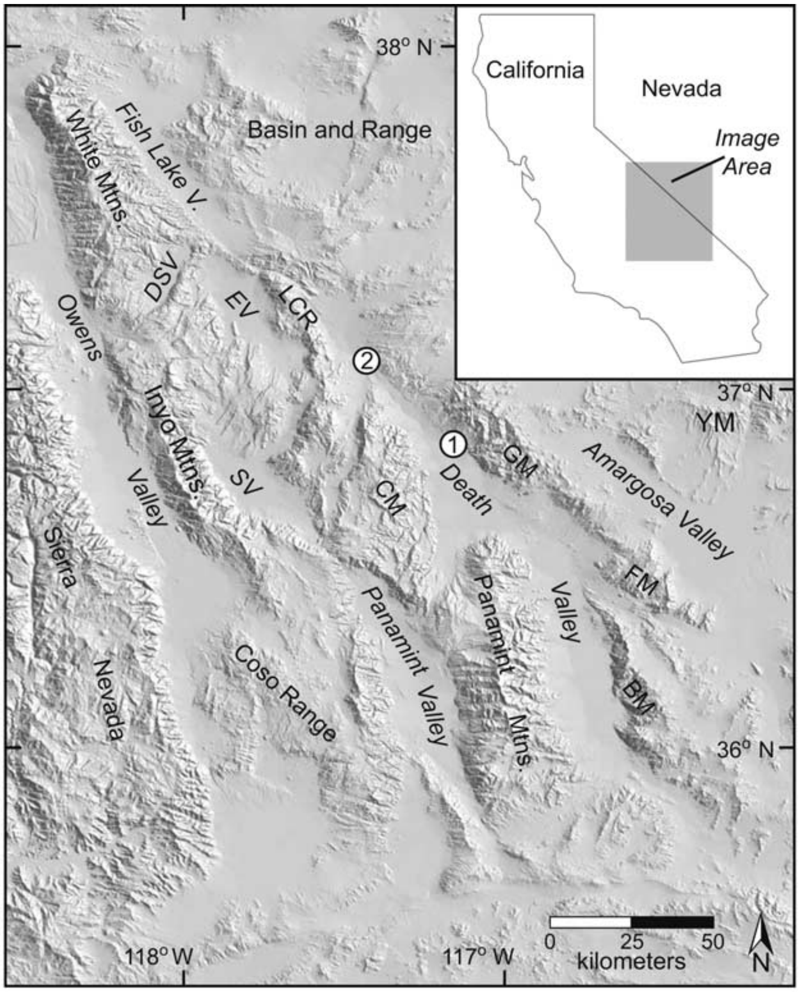

Figure 1. Location map of the study sites and surrounding areas. Circled numbers represent the locations of the two alluvial fans in northern Death Valley used in this study. Location 1 refers to the fan in Figures 2a and 3. Location 2 refers to the fan in Figures 2b and 4. DSV, Deep Springs Valley; EV, Eureka Valley; LCR, Last Chance Range; GM, Grapevine Mountains; CM, Cottonwood Mountains; SV, Saline Valley; FM, Funeral Mountains; BM, Black Mountains; YM, Yucca Mountain.

unprecedented detail [*Carter et al.*, 2001, 2003]. The high resolution of ALSM digital topographic data, generally on the order of 0.5 to 3 m in the horizontal and 10 to 20 cm vertically, allows the construction of very accurate digital elevation models, from which a number of surface characteristics can be readily extracted [*Krabill et al.*, 1995; *Shrestha et al.*, 1999; *Carter et al.*, 2003; *Haugerud et al.*, 2003]. Of particular interest to differentiating and quantifying alluvial landform development is surface roughness, which is often one of the most obvious features distinguishing fans of different age, yet has traditionally been one of the hardest metrics to quantify.

[6] Previous studies using ALSM digital elevation data to differentiate, characterize, and map landslide morphology have shown that surface roughness may be evaluated in a variety of ways [*McKean and Roering*, 2004; *Glenn et al.*, 2006]. *McKean and Roering* [2004] analyzed ALSM data to objectively map the spatial and temporal characteristics of a landslide in New Zealand on the basis of topographic roughness determined by eigenvector ratios. In a similar study, based on various measures of topographic roughness, *Glenn et al.* [2006] used surface roughness, slope, semivariance, and fractal dimension to characterize and differentiate landslide morphology and activity. In addition, *Staley et al.* [2006] used ALSM data to investigate depositional patterns on small debris flow fans in central Death Valley through the analysis of profile curvature and fan gradient.

[7] Here we use the classic methods of topographic variability, degree of varnish accumulation, soil development, and clast size counts, combined with a quantitative measure of surface roughness calculated as the standard deviation of slope from ALSM data, to characterize and differentiate alluvial fan surfaces with different relative ages. Our calculation of surface roughness differs from previous studies in that it allows us to investigate topographic patterns at scales of individual bars and swales to entire alluvial fan systems. Specifically, this study is focused on two alluvial fan complexes in northern Death Valley, along the western Grapevine Mountains piedmont (Figures 1 and 2). We show that fan units of different relative age can be successfully delimited through statisti-

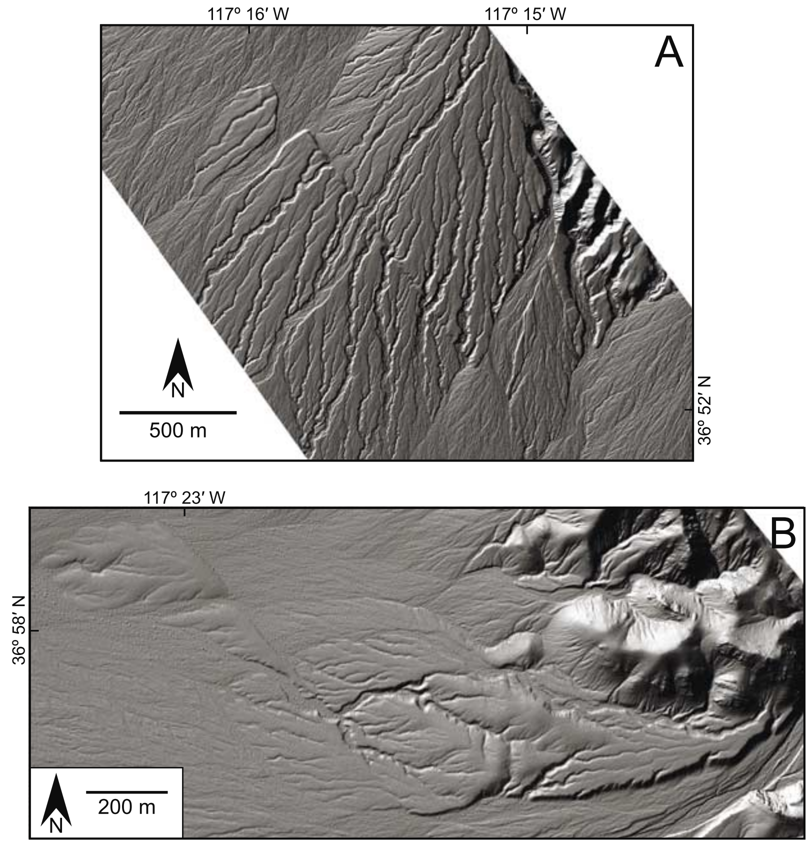

Figure 2. Hill-shaded relief maps derived from airborne laser swath mapping data of the two alluvial fans in northern Death Valley analyzed in this study. Images were produced by gridding the airborne laser swath mapping data at 1 m and fitting a surface through a kriging routine. (a) Alluvial fan at location 1 in Figure 1. (b) Alluvial fan at location 2 in Figure 1.

cally unique surface roughness values extracted from high-resolution ALSM data and propose a model for the evolution of alluvial surfaces through time on the basis of the surface roughness calculations. Furthermore, our results suggest that ALSM data can be used to efficiently and objectively map alluvial landforms.

2. Geologic Setting

[8] Death Valley is located along the western edge of the Great Basin, at the transition between the extensional Basin and Range Province and the strike-slip faults comprising the eastern California shear zone. Death Valley is a pull-apart basin formed by a step-over between the right-lateral southern Death Valley and northern Death Valley fault zones. Displacement along a down-to-the-west normal fault forms the deep, central basin between the two strike-slip fault systems [*Burchfiel and Stewart*, 1966]. Opening of the basin as a result of continued tectonic activity since at least the Miocene has produced the accommodation space necessary for continuous deposition of alluvial deposits [*Hamilton*, 1988; *Wernicke et al.*, 1988; *Burchfiel et al.*, 1995]. Rates of tectonic activity range from 1 to 3 mm/yr along the normal fault in central Death Valley to ~4.5 mm/yr on the northern Death Valley fault zone [*Brogan et al.*, 1991; *Klinger*, 2001; *Knott et al.*, 2002; *Frankel et al.*, 2007].

[9] Climate in the region during late Pleistocene and Holocene time has been dominated by two wet, cold periods and two warm, dry intervals [*Li et al.*, 1996; *Lowenstein et al.*, 1999]. Perennial lakes existed in the central basin during the penultimate glacial advance from ~128 to 186 ka (oxygen isotope stage 6) and the last glacial maximum from ~12 to 35 ka (oxygen isotope stage 2) when the climate was cooler and wetter [*Lowenstein et al.*, 1999]. From 60 to 120 ka, climate is thought to have been similar to the aridity characterizing the Holocene environment [*Lowenstein et al.*, 1999]. The period from 35 to 60 ka was a time of unstable climate and hence, fluctuating lake levels. The present-day arid climate results from the large rain shadow produced by the Sierra Nevada, Inyo Mountains, and Panamint Mountains (Figure 1) [*Poage and Chamberlain*, 2002]. With elevations up to ~4400 m, these three ranges inhibit the eastward migration of moist air masses coming from the Pacific Ocean. As a result, modern-day precipitation in central Death Valley is a sparse ~6 cm/yr (Western Region Climate Center, http://www.wrcc.dri.edu).

3. Alluvial Fan Stratigraphy and Surface Characteristics

[10] Alluvial fans are pervasive piedmont features at the base of the major mountain ranges bounding Death Valley

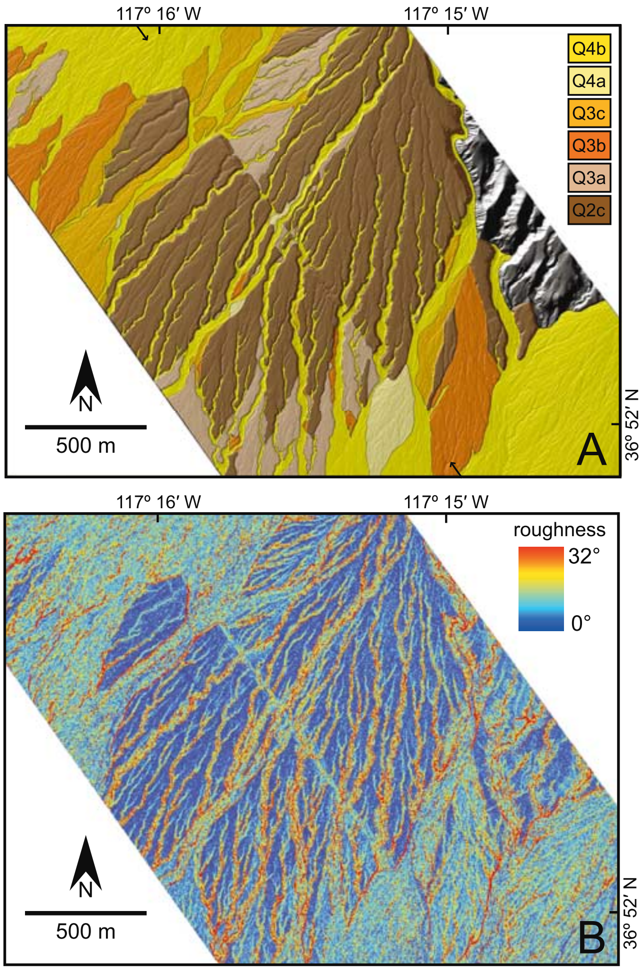

Figure 3. Geologic and surface roughness maps of the alluvial fan at location 1 in Figure 1. (a) Surficial geologic map of the alluvial fan. Arrows delineate the trace of the dextral-slip northern Death Valley fault zone [*Frankel et al.*, 2007]. Faults are left off map for clarity. See text and Table 1 for detailed descriptions of map units. Modified from *Klinger* [2001]. (b) Surface roughness map of the alluvial fan in Figure 3a. Roughness values were calculated as the standard deviation of slope over a 5 m^2 area. Note the similarity with the geologic map in Figure 3a. Scale bar represents values of the standard deviation of slope, which is the metric used in this study to measure surface roughness.

to the east and west (Figures 1 and 2). Relatively small, steep alluvial fans deposited mainly in debris flow events are found at the base of the Black Mountains, where they are commonly offset by the range-bounding normal fault [*Denny*, 1965; *Brogan et al.*, 1991; *Burchfiel et al.*, 1995; *Staley et al.*, 2006]. Throughout much of the rest of the Death Valley basin, such as along the eastern Panamint and western Funeral and Grapevine Mountains piedmonts (Figures 1 and 2), alluvial fans are spatially more extensive, forming continuous bajada-like surfaces. Alluvial fans in these locations are generally thought to be deposited through a combination of sheet-wash and debris flow events [*Denny*, 1965; *Hunt and Mabey*, 1966; *Bull*, 1977; *Blair*, 2000].

[11] Previous work, both in Death Valley and throughout southwestern North America, has defined a consistent alluvial fan stratigraphy for the region [*Denny*, 1965; *Hunt and Mabey*, 1966; *Moring*, 1986; *Bull*, 1991; *Klinger*, 2001]. The alluvial fans in our two study areas comprise eight distinct lithostratigraphic units: Q4b, Q4a, Q3c, Q3b, Q3a, Q2c, Q2b, and Q2a (Figures 3 and 4). Unit Q4b represents active alluvial channels and occupies the lowest topographic position in the landscape. Unit Q2a is the oldest alluvial landform in the study area and thus stands topographically higher than the other units (Figures 3 and 4). Each of these units is described briefly below. More detailed descriptions of the alluvial fan stratigraphy can be found in the works of *Bull* [1991] and *Klinger* [2001, 2002]. In addition, we measured clast sizes at 1-m increments for 50 m on each surface in the midsection of the fans to further characterize the units on the basis of field observations. Table 1 provides a synopsis of the characteristics of each of the mapped surfaces in the study area.

3.1. Q4b

[12] This is the youngest surface mapped in the study area (Figure 3a) and is defined as the active alluvial fan channels. The alluvium in this deposit is generally distributed bimodally, with bars of coarse cobbles and boulders, and swales (channels) consisting of finer-grained pebbles and sand (Figures 5a and 6). No desert varnish, soil, or desert pavement are developed on this surface. Relief on this surface ranges from 0.5 to 1.5 m.

3.2. Q4a

[13] The Q4a surface (Figure 3a) is characterized by prominent bar and swale topography similar to that of unit Q4b, with clasts ranging from pebble to boulder in size (Figures 5b and 6). Little to no varnish or rubification is developed on clasts. Locally, immature patches of pavement are observed in small, ~4 to 6 m^2 areas. The Q4a surface commonly has a thin (up to 5 cm thick), Av soil horizon. This unit is the most recently abandoned surface found on the alluvial fans and is generally 0.5 to 1 m above the active channels.

3.3. Q3c

[14] A distinct bar-and-swale topography is still present on the Q3c surface with 0.5 to 1.0 m of relief (Figure 3a), however, an immature pavement, composed mainly of finer-grained clasts has started to form (Figure 5c). In addition, clasts, which range in size from pebbles to boulders (Figure 6), have a light coating of varnish and are slightly rubified. A weakly developed soil is present beneath the surface and is defined by a ≤5-cm-thick Av horizon, and a ~15-cm-thick B horizon with minor salt (Stage I), carbonate, and clay-film accumulations.

3.4. Q3b

[15] The Q3b surface (Figure 3a) is characterized by an intermediate desert pavement and a bar-and-swale morphology with moderate relief of 0.25 to 0.75 m (Figure 5d). Clasts, which range in size from pebbles to large cobbles/small boulders (Figure 6), are moderately varnished and rubified. Soils are characterized by a ≥10-cm-thick Av horizon, a ~30-cm-thick B horizon with small amounts of

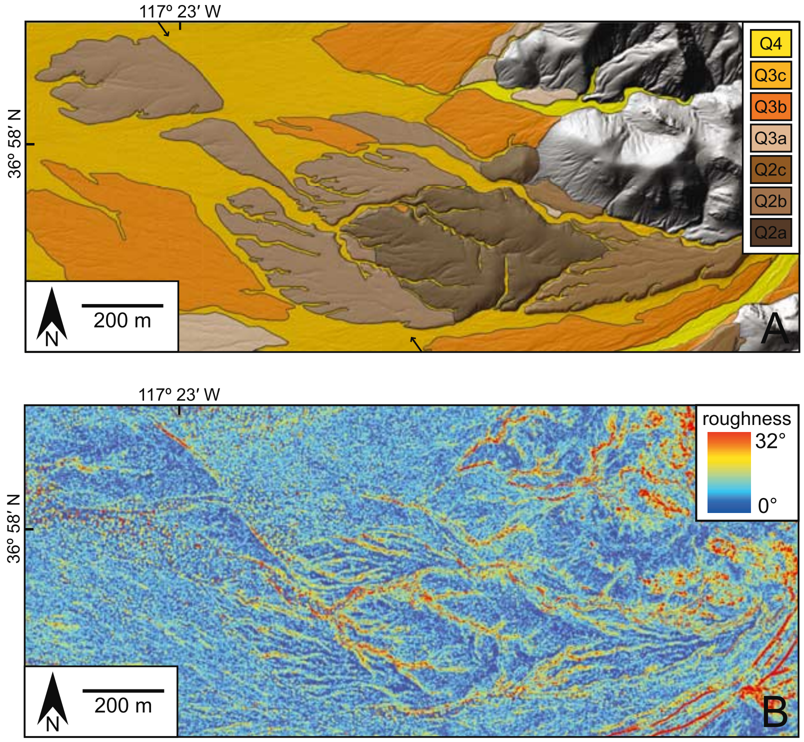

Figure 4. Geologic and surface roughness maps of the alluvial fan at location 2 in Figure 2. (a) Surficial geologic map of the alluvial fan. Arrows delineate the trace of the dextral northern Death Valley fault zone. Faults are left off map for clarity. See text and Table 1 for detailed descriptions of map units. (b) Surface roughness map of the alluvial fan in Figure 4a. Note the similarity with the geologic map in Figure 4a. Roughness values were calculated as the standard deviation of slope over a 5 m^2 area. Scale bar represents values of the standard deviation of slope, which is the metric used in this study to measure surface roughness.

salt and carbonate accumulations (Stage I+) and moderate clay film development. In addition, weak soil development, ~10 cm thick, has altered the C horizon.

3.5. Q3a

[16] The bar-and-swale topography on the Q3a surface (Figure 3a) is subdued (0.1 to 0.5 m of relief), yet still observable, with clasts ranging from pebbles to cobbles in size (Figures 5e and 6). The surface is characterized by a well-packed pavement and clasts that are moderately to heavily varnished and rubified. A moderately well-developed soil is found beneath the surface and is distinguished by a 10- to 20-cm-thick Av horizon, a 40- to 50-cm-thick B horizon with Stage II salt and carbonate accumulations, and a weakly developed C horizon.

3.6. Q2c

[17] Clasts on the Q2c surface (Figure 3a) range from cobbles to small boulders in size (Figure 6). The clasts are tightly packed and form a mature desert pavement. The

Table 1. Northern Death Valley Alluvial Fan Characteristics

Unit	Desert Pavement Development	Bar and Swale Structure		Clast Size Distribution,[a] cm			Surface Roughness, σ_m			Number of Roughness Measurements Extracted
		Morphology	Relief, m	Min.	Max.	Mean	Min.	Max.	Mean	
Q4b	none	prominent	0.5 to 1.5	2	85	16	0.41	15.28	3.55	14129
Q4a	none/immature	prominent	0.5 to 1.25	2	65	17	0.35	7.78	1.89	5525
Q3c	immature/moderate	well-defined	0.5 to 1.0	1	78	15	0.33	10.77	1.94	9813
Q3b	moderate	subdued	0.25 to 0.75	2	52	9	0.29	6.5	1.59	10054
Q3a	mature	subdued	0.1 to 0.5	2	12	5	0.12	3.51	1.02	6012
Q2c	mature	none	0	2	20	7	0.16	5.16	0.71	12747
Q2b	moderate/mature	none/subdued	0 to 0.25	2	13	7	0.20	3.15	0.97	7264
Q2a	moderate/mature	none/subdued	0 to 0.25	4	55	9	0.21	3.73	1.08	7350

[a]Clast size distributions were determined from a count of 50 clasts at one clast/meter for a 50-m segment of each surface in the midsection of the alluvial fan.

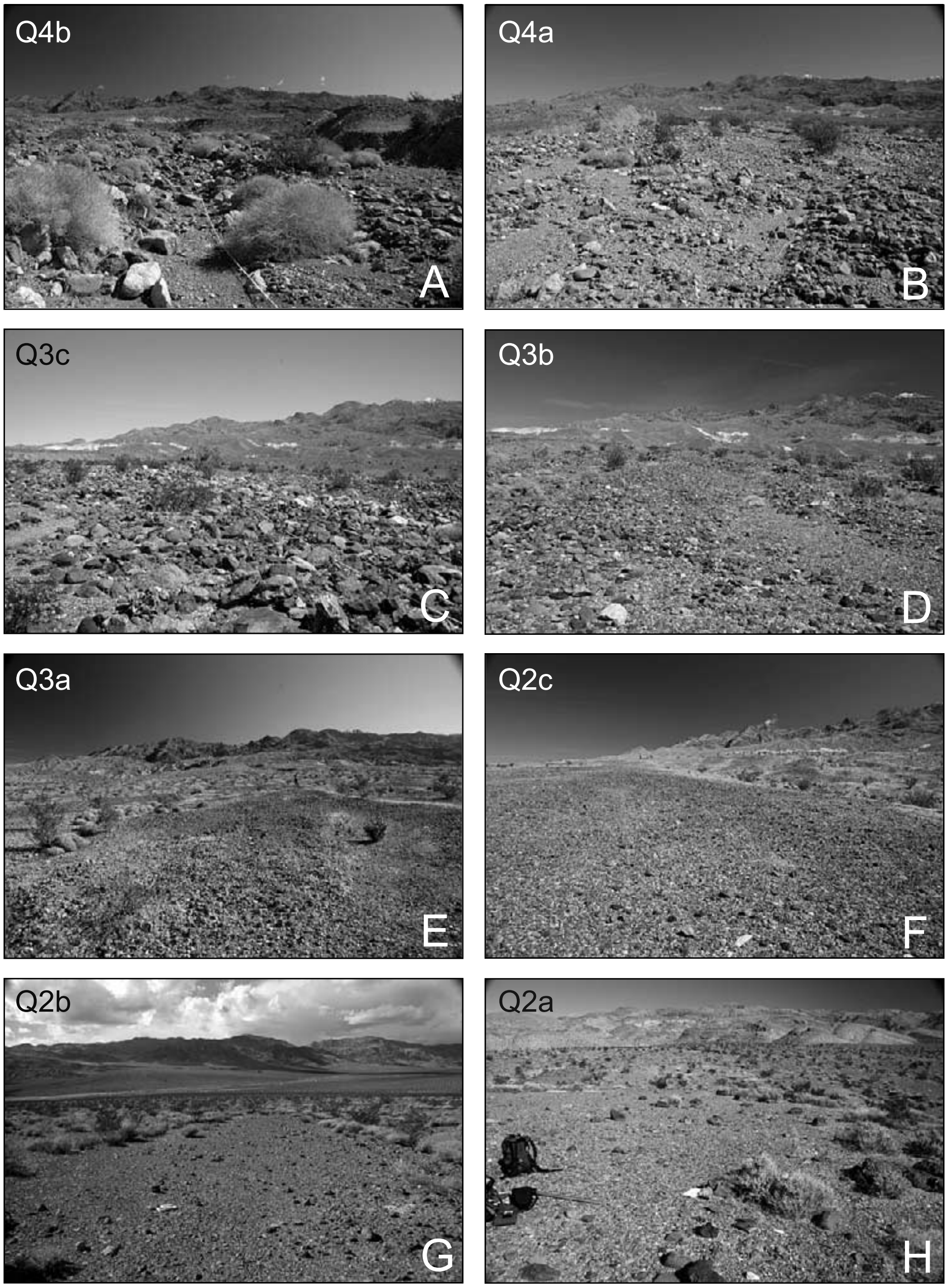

Figure 5. Photographs showing examples of the eight alluvial fan units mapped in northern Death Valley. (a) Unit Q4b. (b) Unit Q4a. (c) Unit Q3c. (d) Unit Q3b. (e) Unit Q3a. (f) Unit Q2c. (g) Unit Q2b. (h) Unit Q2a. Note the progression from the prominent bar and swale topography of the youngest units in Figures 5a, 5b, and 5c to the planar intermediate-age surface in Figure 5f and the more rounded surfaces in Figures 5g and 5h. See Table 1 and text for more detailed descriptions of each unit.

morphology of the Q2c unit is characterized by highly subdued to nonexistent bar-and-swale morphology (Figure 5f). Tops of clasts are heavily varnished and clast undersides are highly rubified. Beneath the Q2c surface a 50+-cm-thick soil is developed. The soil is characterized by a 10- to 20-cm-thick Av horizon with clay film accumulation in its lower half; a middle Bt horizon with carbonate and salt development; and lower Bk horizon with moderate carbonate accumulation (Stage III). The Q2c surface in our study area is ~70 ka, based on ^{10}Be and ^{36}Cl cosmogenic nuclide surface exposure geochronology [*Frankel et al.*, 2007].

3.7. Q2b

[18] The Q2b unit (Figure 4a) is characterized by smooth pavements that are moderately dissected, forming rounded hillslopes. The surface of the Q2b unit generally has a subdued bar-and-swale morphology with 0 to 0.25 m of local relief (Figure 5g). Clasts range in size from pebbles to

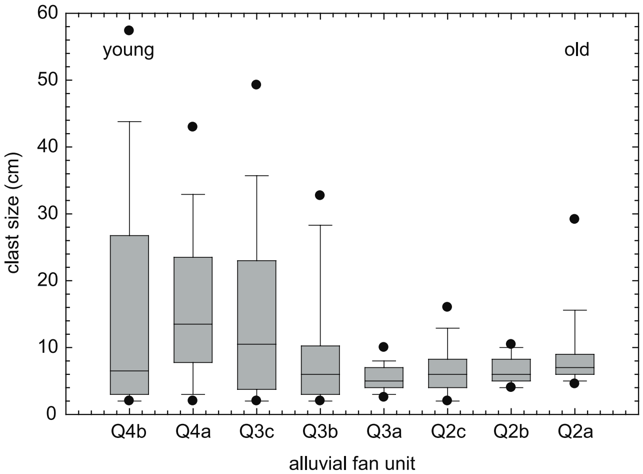

Figure 6. Box and whisker plot of clast sizes from each alluvial fan unit in the study area. Clast counts were conducted by measuring the clast size at 1-m increments for 50 m on each surface in the midsection of the fan. A total of 50 clasts were measured on each surface. Horizontal bar in the center of the box represents the mean clast size. The limits of each box are the 25th and 75th percentiles. Whiskers (bars extending from the boxes) define the 10th and 90th percentiles and the black dots represent the 5th and 95th percentiles for clast sizes in each unit.

small boulders and are packed together in a moderately- to well-developed pavement (Figure 6). Varnish development is generally moderate to high and clasts are highly rubified. A mature soil is developed beneath the Q2b surface and is characterized by a 10- to 20-cm-thick Av horizon, a 20- to 60-cm-thick Bt horizon, and a 50- to 100-cm-thick Bk horizon with Stage III carbonate development.

3.8. Q2a

[19] This unit is the oldest surface analyzed in our study (Figure 4a). The Q2a surface is generally composed of the incised remains of pavements forming convex hillslopes (Figure 5h). Clasts range in size from pebbles to boulders and are generally moderately varnished and moderately to heavily rubified (Figure 6). Soil formed beneath the surface is characterized by a 10- to 20-cm-thick Av horizon, a Bt horizon up to 100 cm thick, and a 100- to 200-cm-thick Bk horizon with Stage IV carbonate development. Where bar and swale topography is present on this surface it is generally subdued, having relief on the order of 0 to 0.25 m.

[20] Each of these units is identifiable and mappable from both field observations and high-resolution ALSM digital topographic data. In addition, individual units possess a distinct topographic signature, which can be readily extracted from ALSM data to quantify the dominant geomorphic characteristics of these deposits.

4. Airborne Laser Swath Mapping

[21] Airborne laser swath mapping (ALSM) digital topographic data have several advantages over more common forms of "static" remote sensing technology such as aerial photographs or satellite imagery. ALSM data can be manipulated in a geographic information system to extract features from the landscape such as elevation, slope, aspect, and curvature, among others. Moreover, detailed surveying of landforms, which takes days to weeks with traditional methods, can be accomplished in a matter of hours with ALSM data.

[22] The ALSM data used in this study were acquired by the National Center for Airborne Laser Mapping at the University of Florida [*Carter et al.*, 2001] using a Cessna 337 twin-engine aircraft equipped with a Optech Model ALTM 1233 laser mapping system. The 33 kHz laser source was flown over the southern part of the study area (location 1 in Figure 1) at an elevation of 600 m above ground level and at an elevation of 820 m above ground level over the northern study site (location 2 in Figure 1) at an average speed of 60 m/s. The difference in elevation between the two study sites is a function of the amount of topographic relief along the range-front in each region and does not affect the final resolution of the data. First and last returns, as well as the intensity of each laser pulse, were recorded. The sparse vegetation in the study area is ideal for ALSM data acquisition because the removal of data points related to laser returns from the tops of flora does not reduce the point density of bare-earth shots, as it might in a heavily canopied region. Individual bare-earth data points were aligned in an equally spaced grid at 1-m intervals and fit with a smooth surface through a kriging algorithm using Surfer software. This produced a digital elevation model from the rasterized grid with 1-m horizontal resolution and 5- to 10-cm vertical accuracy [e.g., *Krabill et al.*, 1995; *Burroughs and McDonnell*, 1998; *Shrestha et al.*, 1999; *Carter et al.*, 2001, 2003; *Sartori*, 2005; *Chaplot et al.*, 2006]. The grid was then imported into ArcInfo, which was used for all topographic analyses.

5. Surface Roughness

[23] Surface morphology is one of the most widely used criteria to distinguish alluvial fans of different ages [e.g., *Wells et al.*, 1987; *Bull*, 1991; *Ritter et al.*, 1993]. Previous studies suggest that the relative age of alluvial deposits is manifested by topographic variability, with fan surfaces tending to become smoother with increasing age [*Bull*, 1977, 1991; *Matmon et al.*, 2006]. We exploit the high resolution of ALSM-derived digital elevation models to quantify changes in alluvial fan surface roughness through time. Although there are many ways in which to measure the texture of alluvial and colluvial material [e.g., *McKean and Roering*, 2004; *Glenn et al.*, 2006], we define surface roughness as the standard deviation of slope. We choose to calculate the roughness metric in this way because it allows us to average out surface features over a 5 m by 5 m area, thereby eliminating any anomalies related to individual boulders or the occasional large creosote bush. Furthermore, taking this approach to calculating surface roughness accounts more readily for the wavelengths (~5 to 10 m) of bar and swale morphology that are commonly observed in arid alluvial environments.

5.1. Standard Deviation of Slope

[24] The standard deviation of slope was calculated by first deriving a slope map from the 1-m-resolution, ALSM-derived digital elevation model. Slope, m, is defined for the

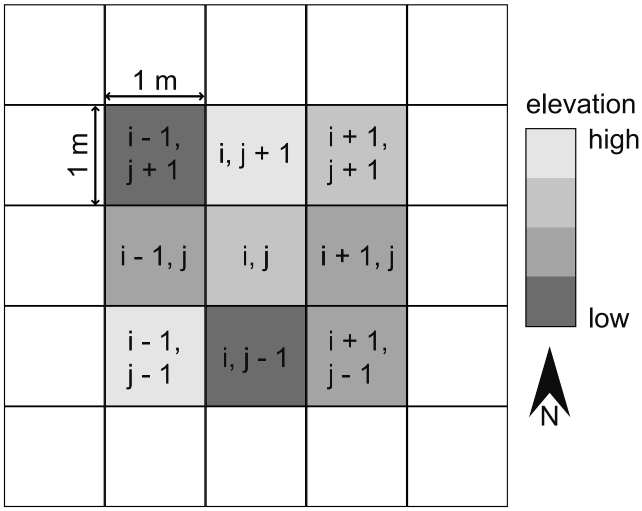

Figure 7. Schematic diagram of a 3 m by 3 m window in which slope and standard deviation of slope values are determined. Each cell is 1 m by 1 m in size. Slopes for the 3 m by 3 m window are calculated for the central cell (i, j) in the moving window. Slopes are calculated as the maximum difference between cells in the east-west and north-south directions. See text and equations (1), (2), and (3) for details. The standard deviation of slopes (σ_m) is taken as the standard deviation of all nine cells in the window and is reported in the center cell (i, j) of each window. See text and equation (4) for details.

central cell in a 3 m by 3 m (three cell by three cell; cell i, j in Figure 7) moving window as

$$m = \tan^{-1}\sqrt{\left(\frac{\partial z}{\partial x}\right)^2 + \left(\frac{\partial z}{\partial y}\right)^2}, \tag{1}$$

where

$$\frac{\partial z}{\partial x} = \frac{\left[\left(z_{i+1,j+1} + 2z_{i+1,j} + z_{i+1,j-1}\right) - \left(z_{i-1,j+1} + 2z_{i-1,j} + z_{i-1,j-1}\right)\right]}{8\partial x} \tag{2}$$

$$\frac{\partial z}{\partial y} = \frac{\left[\left(z_{i+1,j+1} + 2z_{i,j+1} + z_{i-1,j+1}\right) - \left(z_{i+1,j-1} + 2z_{i,j-1} + z_{i-1,j-1}\right)\right]}{8\partial y}. \tag{3}$$

Here $\partial z/\partial y$ is the maximum slope in the north-south direction, $\partial z/\partial x$ is the maximum slope in the east-west direction, z is the elevation at a cell location specified by the subscripts relating to the schematic diagram in Figure 7, and ∂x and ∂y are the east-west and north-south cell dimension [*Horn*, 1981; *Burroughs and McDonnell*, 1998]. In our example, the north-south and east-west cell dimensions are everywhere 1 m.

[25] The standard deviations of slope values are then calculated in a moving window over the slope map, where the standard deviation values are reported in the central cell (cell i, j in Figure 7). We define standard deviation as

$$\sigma_m = \sqrt{\frac{\sum_{i=1}^{n}(m_i - \overline{m})^2}{n}}, \tag{4}$$

where σ_m is the standard deviation of slope or surface roughness, n is the number of samples in the population, which in our analysis ranges from nine samples for a three cell by three cell area to 40,000 samples for a 200 cell by 200 cell region, m_i is the value of one specific sample within the sampling area, and $\overline{m}$ is the population mean [*Taylor*, 1997]. Because slope values are determined across a 3 m by 3 m window and σ_m values are computed from a subsequent filter of the slope map, surface roughness is averaged over areas ranging from a 5 m^2 area for a three cell by three cell moving window to a 202 m^2 area for a 200 cell by 200 cell window.

5.2. Surface Roughness Results

[26] Approximately 73,000 individual σ_m values were extracted from the eight mapped fan units in the study area for each standard deviation window size (Table 1). Points were collected from the center of representative portions of each surface to avoid anomalously high surface roughness values associated with parts of the landscape such as the steep channel walls incised through the fans (Figures 3 and 4). These data illustrate the distinct character of each surface and reveal a trend of decreasing roughness with increasing age when roughness is analyzed over a 5 m^2 area (Figure 8). On the oldest surfaces, this pattern is reversed, with surface roughness and age becoming positively correlated on the

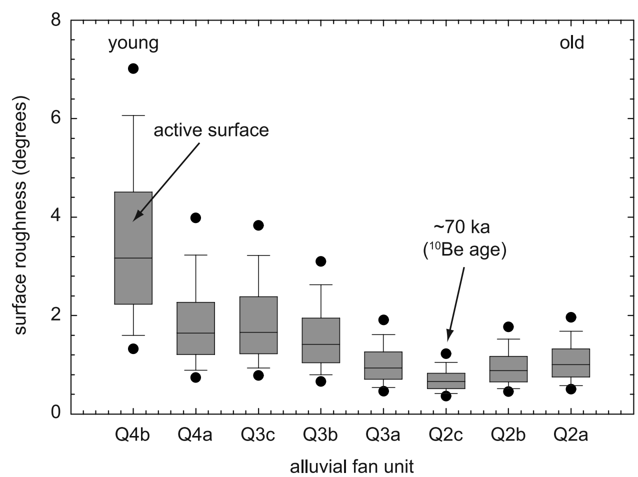

Figure 8. Box and whisker plot of surface roughness averaged over 5 m^2 for each alluvial fan unit in the study area. The horizontal bar inside each box is the mean. Box limits represent the 25th and 75th percentiles. Whiskers (bars extending from the top and bottom of each box) are the 10th and 90th percentiles and the black dots represent the 5th and 95th percentiles. Note the pattern of surfaces smoothing out with age and then starting to become rougher again as age increases further. The age of the Q2c surface is from ^{10}Be and ^{36}Cl cosmogenic nuclide surface exposure geochronology [*Frankel et al.*, 2007].

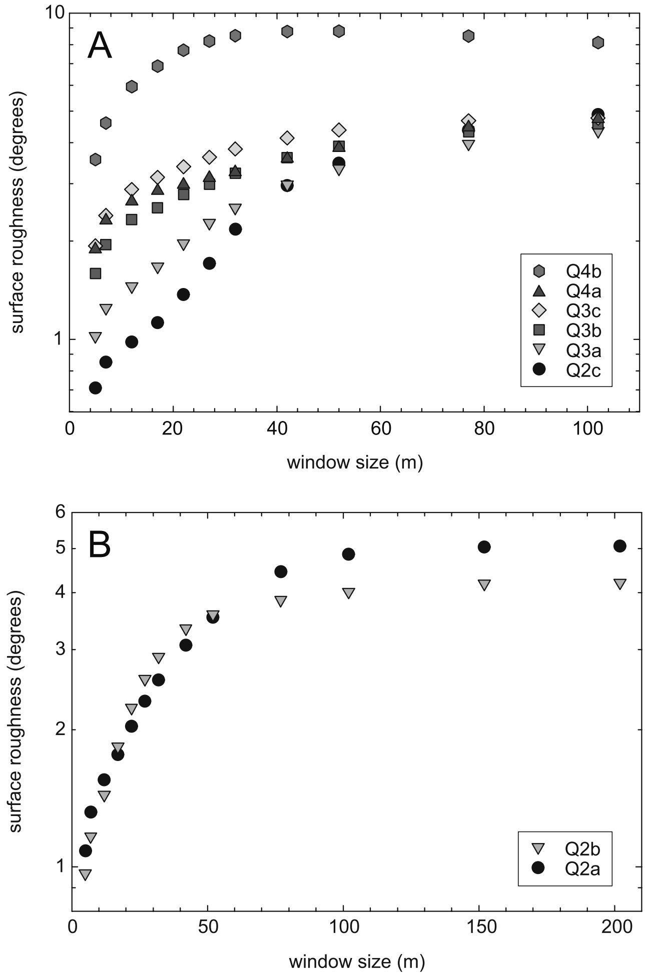

Figure 9. Plots showing mean surface roughness versus window size used to calculate the standard deviation of slope values. (a) Mean surface roughness versus size of moving window for the Q4b, Q4a, Q3c, Q3b, Q3a, and Q2c surfaces. Window size ranges from 5 m by 5 m to 102 m by 102 m. (b) Plots of mean surface roughness versus window size for the Q2a and Q2b surfaces. Window sizes range from 5 m by 5 m to 202 m by 202 m. Dominant surface roughness wavelengths are represented by the steepest parts of the curves. Roughness on the youngest surfaces is characterized at wavelengths of bar and swale topography (Figure 9a). Older surfaces have topographic signatures that are defined by the longer wavelengths of convex hillslopes incised by tributary channels. See text for further discussion.

oldest fan deposits in the study area (Figure 8). In addition, younger surfaces exhibit a higher variance in surface roughness values, which progressively decreases with increasing age (Figure 8).

[27] When compared with previously mapped alluvial fan units in northern Death Valley (Figures 3a and 3b), maps of σ_m values across the study area clearly illustrate the utility of this metric in characterizing and defining individual lithostratigraphic units (Figures 3b and 4b). Most prominent among these is the Q2c surface, which is the smoothest and most stable alluvial landform in the region (Figure 3b). Other alluvial units, although not as well defined, are still clearly distinguishable when compared with geologic observations (Figures 3 and 4).

[28] Calculation of surface roughness at multiple length scales (i.e., by determining σ_m in moving windows of different size) also brings out a number of interesting patterns in the landscape (Figure 9). When mean surface roughness is plotted against the size of the moving window over which those values are determined, each surface is characterized by an initial increase in surface roughness with increased window size (Figure 9). Eventually each unit reaches a point where roughness no longer increases as a function of window size (e.g., "interface width" of *Barabasi and Stanley* [1995]) and roughness values eventually converge at the longest length scales (Figure 9a). In general, individual surfaces have distinct saturation lengths, with an increase in length scale corresponding to an increase in surface age (Figure 9).

5.3. Statistical Analysis

[29] Although the values of surface roughness on each of the eight alluvial fan units appear to be derived from unique populations (Figure 8), we quantitatively test this supposition using a Kolmogorov-Smirnov test. The Kolmogorov-Smirnov test was chosen because it does not make any assumptions regarding the distribution of sample populations, allows populations of different size to be directly compared to one another, and is most effective when applied to large ($n \geq 40$) data sets [*Borradaile*, 2003]. The test relies on the maximum difference between the cumulative frequency distributions of two sample populations (Figure 10 and auxiliary material Figure S1[1]),

$$D = \max(|F1(x) - F2(x)|), \tag{5}$$

where D is the Kolmogorov-Smirnov test statistic (D statistic), and $F1(x)$ and $F2(x)$ are the cumulative frequency distributions of two sample populations [*Davis*, 2002]. D is compared against a critical value, D_α, for a given level of significance defined as

$$D_\alpha = f_\alpha \sqrt{N}, \tag{6}$$

where

$$N = \sqrt{\frac{n_1 + n_2}{n_1 n_2}} \tag{7}$$

and f_α is a coefficient specific to the confidence level for the critical value of D_α. The f_α coefficient is equal to 1.36 for the 95% confidence level and 1.63 for the 99% confidence level. n_1 and n_2 are simply the number of samples in the cumulative distribution functions, $F1(x)$ and $F2(x)$ [*Chakravarti et al.*, 1967; *Borradaile*, 2003].

5.4. Kolmogorov-Smirnov Test Results

[30] Kolmogorov-Smirnov analyses ultimately test for the existence of a null hypothesis. Here the null hypothesis is that surface-roughness values for each mapped alluvial fan unit (Figures 3 and 4) are derived from the same sample population. Each mapped alluvial fan surface was compared to the two surfaces adjacent to it in terms of relative age

[1]Auxiliary materials are available in the HTML. doi:10.1029/2006JF000644.

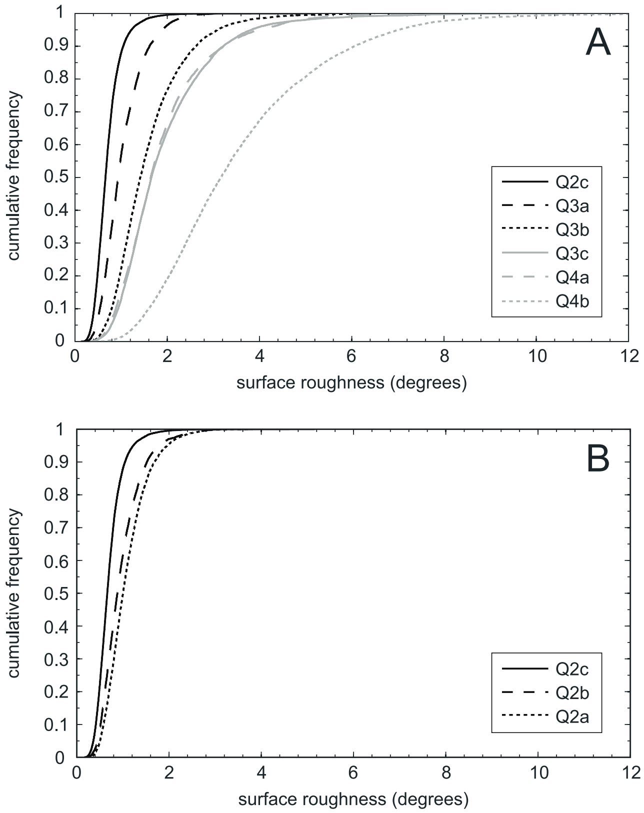

Figure 10. Cumulative frequency distributions of surface roughness (σ_m) determined in a 5 m by 5 m moving window for the comparison of eight alluvial fan units in northern Death Valley. The D statistic in the Kolmogorov-Smirnov test is the maximum difference between the cumulative frequency distributions of two sample populations (equation (5)). (a) Cumulative frequency distributions for units Q4b to Q2c. (b) Cumulative frequency distributions for units Q2c to Q2a. See text and Table 1 for descriptions of each unit.

(Table 2). For example, unit Q3b was compared to both Q3c and Q3a, its younger and older neighbors, respectively. In addition, units that appeared to have similar σ_m distributions, yet were not adjacent to one another in terms of relative age, such as units Q2b and Q3a, were also compared. Figures 10 and 11 show the relationship between fan units based on the Kolmogorov-Smirnov D statistic and normalized for the size of each population (Table 1).

[31] Comparison of each mapped unit on the basis of the surface roughness calculations averaged over a 5 m^2 area clearly illustrates that the alluvial fan units defined in northern Death Valley are derived from populations that are statistically unique at the 99% confidence interval (Table 2 and Figure 11). We can therefore reject the null hypothesis that samples from individually mapped units are derived from the same populations.

Table 2. Kolmogorov-Smirnov Test Results

Alluvial Fan Unit Comparison	Significance Level, α[a]	P Value[b]	D Statistic[c]	N, n_1+n_2/n_1n_2[d]
Q2a versus Q2b	0.01	1.5×10^{-49}	0.1242	0.000274
Q2b versus Q2c	0.01	0	0.304	0.000216
Q2c versus Q3a	0.01	0	0.3704	0.000245
Q3a versus Q3b	0.01	0	0.3604	0.000266
Q3b versus Q3c	0.01	8.8×10^{-82}	0.1371	0.000201
Q3c versus Q4a	0.01	5.4×10^{-4}	0.0340	0.000283
Q4a versus Q4b	0.01	0	0.4941	0.000252
Q2a versus Q3b	0.01	0	0.3083	0.000302
Q2b versus Q3a	0.01	8.0×10^{-14}	0.0683	0.000216

[a]This represents a confidence level of 99% ($1 - \alpha$).
[b]The P value is the probability that the null hypothesis (i.e., the likelihood that the two samples came from the same population) is true. If the P value is less than α, then the null hypothesis can be rejected.
[c]The D statistic is the maximum difference between the cumulative frequency plots of two populations.
[d]This is the normalization coefficient for two population sizes, n_1 and n_2.

6. Discussion

6.1. Changes in Surface Roughness

6.1.1. Surface Roughness Controlled by Bar and Swale Topography

[32] Quantifying surface roughness across a high-resolution digital elevation data set shows that individual fan units can be distinguished in a statistically significant

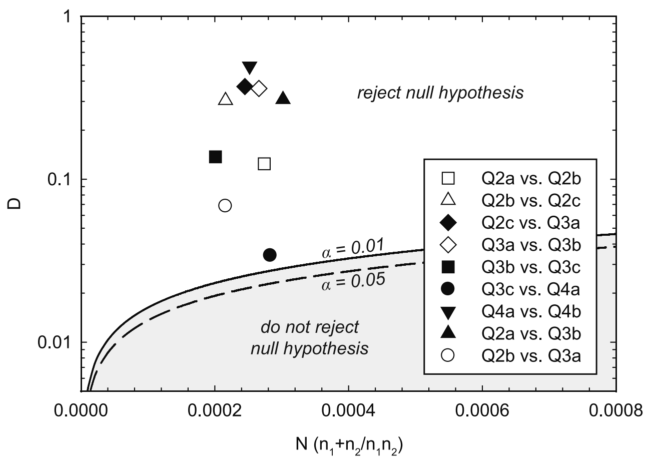

Figure 11. Results of the Kolmogorov-Smirnov tests for the comparison of surface roughness between alluvial fan units at a wavelength of 5 m. Curves represent 95% (α = 0.05) and 99% (α = 0.01) confidence levels. The area above the curves is the region where the null hypothesis of the surface roughness for each unit being derived from the same population can be rejected (i.e., there is a statistically significant difference between the surface roughness of the units compared to one another). The region below the curves shaded in grey represents the region where null hypothesis cannot be rejected and the samples are derived from statistically similar populations. The D statistic on the *y* axis is the maximum difference between the cumulative frequency distributions in Figure 10. The value N on the *x* axis is a normalization parameter for populations of different size where n_1 is the size of one population and n_2 is the size of the population to which n_1 is being compared. See equations (5), (6), and (7) for further explanation. Parameters for the Kolmogorov-Smirnov test can be found in Table 2. Note that surface roughness distributions of units that are adjacent in age, as well as those with similar means but different ages, are all statistically different from each other at the 99% confidence level (α = 0.01).

manner (Figure 11). Surface roughness values, when plotted against relative fan-unit age (Figure 8), bring to light an interesting pattern, which previously has only been described through qualitative field observations [e.g., *Bull*, 1991]. The youngest alluvial fan surfaces, Q4b, Q4a, and Q3c, have the highest surface roughness values (Table 1 and Figure 8). In addition, the youngest surfaces have the largest variance in the surface roughness metric (Table 1 and Figure 8). This pattern results from freshly deposited clasts of different sizes being sequestered into bars and swales. In general, channel bars are composed of larger clasts and swales are filled with finer-grained material (Figure 5).

[33] Inasmuch as relatively coarse-grained alluvium defines bars, and swales comprise finer grains, surface roughness does not vary strictly as a function of clast size. The resolution of the digital elevation model, from which slope values were derived, is 1 m. This window is larger than even the maximum clast size found on any individual fan surface in the study area (Table 1 and Figure 6). Therefore our calculations of surface roughness take into account only the medium wavelength (~5 to 10 m) bar-and-swale structures that dominate the surface morphology of alluvial fans. We note, however, that clast size may influence the formation and preservation of the bar-and-swale structures, as fans tend to be rougher (higher standard deviation of slope) where mean clast sizes are larger, which leads to a higher angle of repose, and where field observations suggest more prominent expression of bar-and-swale morphology (Figures 5, 6, and 8).

[34] As fan surfaces increase in age, surface roughness decreases from the youngest unit, Q4b, to the most stable, smoothest fan surface, Q2c (Figure 8). Previous work defined the age of the Q2c surface to be ~70 ka, on the basis of in situ ^{10}Be and ^{36}Cl cosmogenic nuclide geochronology [*Frankel et al.*, 2007]. Although fan surfaces younger than the Q2c surface have no absolute age control at present, soil formation and varnish accumulation on the Q4 and Q3 deposits suggest that fan smoothing occurs rapidly in the first few thousand years after deposition. From this point until ~70,000 years after deposition, smoothing of the fan surface proceeds ever more slowly with time. On surfaces older than ~70 ka, the steep walls of channels that have incised through the most stable alluvial surface, Q2c, begin to erode by headward tributary incision, and consume the once-planar surface. As this erosion proceeds, the older surfaces, Q2a and Q2b, become increasingly rougher with increasing age as the alluvial fans degrade with time (Figure 8).

6.1.2. Surface Roughness at Multiple Length Scales

[35] Changes in the pattern of surface roughness also occur as a function of the wavelength over which roughness values are calculated (Figure 9). Each mapped fan unit is characterized by an initial, rapid increase in surface roughness corresponding to an increase in the size of the moving window, over which the standard deviation of slope is determined (Figure 9a). The point at which surface roughness no longer changes rapidly as a function of the size of the averaging window gives an indication of the dominant topographic wavelengths for each surface. As the size of the window becomes larger, surface roughness values for each unit converge when the area over which roughness values are calculated begins to incorporate multiple surfaces (Figure 9a).

[36] Units Q4b, Q4a, Q3c, and Q3b are each characterized by a rapid increase in surface roughness values over wavelengths of five to 12 m, representing the typical length scale of bar and swale topography (Figure 9a). At longer wavelengths, surface roughness values increase by only minor amounts, suggesting the topographic saturation length is ~12 m for the youngest surfaces [e.g., *Barabasi and Stanley*, 1995]. We note however, the youngest unit, Q4b, appears to have a saturation wavelength that is somewhat longer than units Q4a, Q3c, and Q3b (Figure 9a). This is likely due to the fact that the Q4b channels are often deeply incised through older alluvial fan surfaces (Figure 3a) and therefore, larger averaging windows incorporate steep channel walls, causing higher standard deviations in slope values. A similar pattern emerges for units Q3a and Q2c.

[37] Units Q3a and Q2c show an initial rapid increase in surface roughness values over wavelengths of 5 to 12 m (Figure 9a). However, both the Q3a and Q2c surface roughness values continue to increase steadily at longer wavelengths (Figure 9a). We feel this also occurs as result of active channels (Q4b) being deeply incised through older surfaces (Figure 3a), thus causing standard deviation of slope values to be higher at longer length scales away from the representative central portion of these deposits.

[38] A somewhat different pattern emerges when surface roughness values are analyzed as a function of window size for the two oldest surfaces in the study area, units Q2b and Q2a (Figure 9b). As with the younger units, surface roughness increases at first, although in this case it occurs over a length scale of 50 to 75 m (Figure 9b). The longer topographic saturation wavelength suggests that roughness values on the older surfaces are no longer controlled by the evolution of bar and swale topography. Rather, increased roughness values on these surfaces are the result of headward incision of tributary channels, transforming the once-planar surfaces into rounded hillslopes, leaving behind a signature of topographic roughness at longer wavelengths. Continued incision of tributary streams causes the oldest surface in the study area, Q2a, to have a longer topographic wavelength than the Q2b deposit.

6.1.3. Clast Size Patterns

[39] A pattern similar to that of surface roughness (Figure 8) is observed in the distribution of clast sizes on fan surfaces (Figure 6). A large range of clast sizes is present on the fan surface immediately following deposition. With time, clasts begin to weather and become buried as fan surfaces smooth out [e.g., *Bull*, 2007]. Absolute clast size and clast-size variance decrease as the fans evolve toward a smooth, stable configuration. As fans continue to increase in age, larger clasts are exhumed from beneath the surface by erosion (Figure 6). Eventually, clast size increases and becomes more variable with age, in much the same way that fan surfaces become rougher.

6.2. Implications for Arid Region Landscape Evolution

[40] Surface roughness, in addition to facilitating the characterization of individual fan units, lends insight to alluvial landform development. We propose an alluvial landform evolutionary scheme that begins with fan deposition within, and downstream from, the mouth of active channels. These areas exhibit prominent bar-and-swale morphology and large variations in clast size. Their surfaces

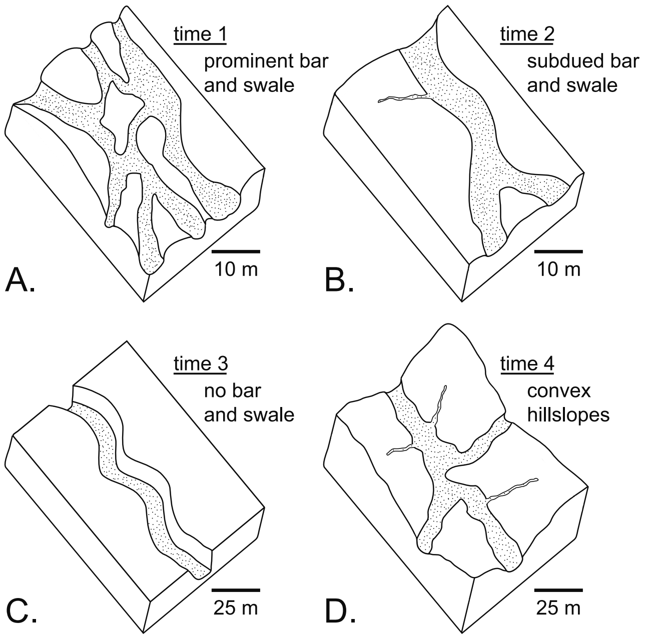

Figure 12. Schematic diagram showing the inferred landform evolution of alluvial fans in northern Death Valley based on surface roughness characteristics. (a) The morphology of a young, active, or recently active, fan surface similar to units Q4b, Q4a, and Q3c with prominent bar-and-swale morphology is shown. Stippled pattern represents active channels and white areas are channel bars with coarser material. (b) Alluvial fan surface where the bar-and-swale morphology has started to smooth out and become subdued is shown. Bars have eroded and filled in channels similar to units Q3b and Q3a. Stippled pattern represents abandoned channel with a concentration of fine-grained sediments. White areas are fan surfaces with moderate pavement development and a reduction in clast size. (c) Smooth, planar alluvial fan surface similar to unit Q2c is shown. White area is characterized by a well-packed, mature pavement and heavy varnish development. Stippled area is an active channel that has incised through the older, smoother surface. (d) As fans continue to increase in age, steep channel walls are eroded by headward incision of tributaries and are transformed into convex (rounded) hillslopes, such as units Q2b and Q2a. In general, pavements are less well developed on these surfaces because of the downslope sediment transport. Stippled areas represent active, or recently active, channels and white areas are the alluvial fan surfaces that are diffusing into more mature landforms.

are rougher than anywhere else in the alluvial fan complex (Figure 12a). Bar and swale topography is formed through a combination of sheet-flood and debris flow events in a braided channel network. The bars result from sediment-rich flows deposited at the end of distributary channels that criss-cross the active fan surface [*Bull*, 1977, 1991; *Harvey and Wells*, 2003]. With time, the locus of deposition changes and the active depositional surface is abandoned. This leaves the surface to evolve into a smooth, stable landform as the undulatory bar-and-swale morphology begins to diffuse away and pavements start to form (Figure 12b). As time progresses, the bar-and-swale structure continues to decay until a highly planar surface with little or no relief is formed (Figure 12c). The smoothing of bar and swale topography results from the winnowing of fine-grained material from bars into swales and the weathering of larger clasts through rain splash, sheet-flow, wind, and expansion and contraction of the Av horizon from cycles of wetting and drying [*Bull*, 1991, 2007]. At the same time, pavements form by surface inflation from aeolian dust deposition and the transport of clasts from bars into swales [*McFadden et al.*, 1987; *Haff and Werner*, 1996; *Haff*, 2001, 2005]. For the case of alluvial fans in the arid environment of northern Death Valley, this is accomplished over a period of ~70,000 years. Eventually, tributary channels form from erosion by surface runoff. Headward incision of these tributaries wears down the steep walls of channels that are incised through the stable, planar surface transforming the oldest alluvial landforms into convex hillslopes [e.g., *Roering et al.*, 1999], leaving only small remnants of the planar surface intact (Figure 12d).

[41] Although the surface-roughness data illustrate the progression of fan development with time, at present we are not able to fully quantify the rates over which these processes operate, with the exception of the $\leq$70 ka it apparently takes to evolve from abandonment of the active depositional surface to a stable, planar landform. A recent study by *Matmon et al.* [2006], in which they investigated the morphologic development of alluvial landforms by measuring cosmogenic nuclide inventories in bars and swales of dated fans, suggests sediment residence times of at least 30,000 years. They suggested that >280,000 years are required for complete smoothing to take place on fans formed along the San Andreas fault in southern California, a significantly longer time interval than we propose for fans in Death Valley. This result emphasizes that rates of alluvial landform evolution are likely to be location-dependent and therefore, calibration for different climatic and tectonic regimes is necessary. Future quantification of the rates of such processes, both through exploitation of high-resolution digital topographic data and by determining the age of individual fan units, will further improve our understanding of postdepositional alluvial landform development.

7. Conclusions

[42] We have exploited the high resolution of ALSM digital topographic data to quantify surface roughness on alluvial fans in northern Death Valley. By calculating surface roughness as the standard deviation of slope in a 5 m by 5 m moving window across a 1-m-resolution digital elevation data set we have shown that individual lithostratigraphic units can be differentiated at the 99% confidence level on the basis of this topographic metric. Additionally, the surface roughness data demonstrate a characteristic, time-dependent evolution of fan morphology that has previously only been described through qualitative field observations. Specifically, the surfaces of alluvial fans decrease in roughness with time, eventually becoming smooth, planar landforms. In the arid climate of Death Valley, this smoothing process appears to occur over a period of $\leq$70,000 years. As the alluvial fan continues to evolve, stable landform configurations eventually erode into convex hillslopes. Once this threshold is crossed, surface roughness increases with age as tributary

channel incision dissects the formerly smooth surface. These results demonstrate that diagnostic morphologic features commonly observed on alluvial deposits can be quantified with high-resolution digital topographic data. With access to high-resolution digital topographic data sets becoming more and more common, this methodology will be a useful aid in the objective identification, mapping, and interpretation of alluvial landforms during future studies.

[43] **Acknowledgments.** This work was supported by the National Center for Airborne Laser Mapping (NCALM), a NASA Earth System Science Fellowship, and the University of California White Mountain Research Station. Permission to conduct research within Death Valley National Park was granted by the Death Valley National Park Service Office of Natural Resources. We thank Lorraine Leon and Hilary Strong for assistance in the field. Discussions with Michael Sartori, Stephanie Briggs, Bill Bull, Ramón Arrowsmith, Bill Carter, Josh Roering, and Ramesh Shrestha are also greatly appreciated. This paper benefited from excellent reviews by Kyle Nichols, Phillip Allen, Alex Densmore, and Robert Anderson.

References

Barabasi, A. L., and H. E. Stanley (1995), *Fractal Concepts in Surface Growth*, 366 pp., Cambridge Univ. Press, New York.

Bierman, P. R., A. R. Gillespie, and M. W. Caffee (1995), Cosmogenic ages for earthquake recurrence intervals and debris flow fan deposition, Owens Valley, California, *Science*, *270*, 447–450.

Birkeland, P. W. (1999), *Soils and Geomorphology*, 372 pp., Oxford Univ. Press, New York.

Blackwelder, E. (1931), Desert plains, *J. Geol.*, *39*, 465–484.

Blair, T. C. (2000), Sedimentology and progressive tectonic unconformities of the sheetflood-dominated Hell's Gate alluvial fan, Death Valley, California, *Sediment. Geol.*, *132*, 233–262.

Borradaile, G. (2003), *Statistics of Earth Science Data*, 351 pp., Springer, New York.

Brogan, G. E., K. S. Kellog, D. B. Slemmons, and C. L. Terhune (1991), Late Quaternary faulting along the Death Valley Furnace Creek fault system, California and Nevada, *U.S. Geol. Surv. Bull.*, *1991*, 23 pp.

Bull, W. B. (1977), The alluvial fan environment, *Prog. Phys. Geogr.*, *1*, 222–270.

Bull, W. B. (1984), Tectonic geomorphology, *J. Geol. Educ.*, *32*, 310–324.

Bull, W. B. (1991), *Geomorphic Responses to Climatic Change*, 326 pp., Oxford Univ. Press, New York.

Bull, W. B. (2007), *Tectonic Geomorphology of Mountains: A New Approach to Paleoseismology*, Blackwell, Malden, Mass., in press.

Burchfiel, B. C., and J. C. Stewart (1966), "Pull-apart" origin of the central segment of Death Valley, California, *Geol. Soc. Am. Bull.*, *77*, 439–442.

Burchfiel, B. C., P. Molnar, P. Zhang, Q. Deng, W. Zheng, and Y. Wang (1995), Example of a supradetachment basin within a pull-apart tectonic setting: Mormon Point, Death Valley, California, *Basin Res.*, *7*, 199–214.

Burroughs, P. A., and R. A. McDonnell (1998), *Principles of Geographical Information Systems*, 356 pp., Oxford Univ. Press, New York.

Carter, W., R. Shrestha, G. Tuell, D. Bloomquist, and M. Sartori (2001), Airborne laser swath mapping shines new light on Earth's topography, *Eos Trans. AGU*, *82*(46), 549.

Carter, W., R. L. Shrestha, and B. Dietrich (2003), National Center for Airborne Laser Mapping proposed, *Eos Trans. AGU*, *84*(30), 281.

Chakravarti, I. M., R. G. Laha, and J. Roy (1967), *Handbook of Methods of Applied Statistics*, 460 pp., John Wiley, Hoboken, N. J.

Chaplot, V., F. Darboux, H. Bourennane, S. Leguedois, N. Silvera, and K. Phachomphon (2006), Accuracy of interpolation techniques for the derivation of the digital elevation models in relation to landform types and data density, *Geomorphology*, *77*, 126–141.

Davis, J. C. (2002), *Statistics and Data Analysis in Geology*, 638 pp., John Wiley, Hoboken, N. J.

Davis, W. M. (1905), The geographical cycle in an arid climate, *J. Geol.*, *13*, 381–407.

Denny, C. S. (1965), Alluvial fans in the Death Valley region, California and Nevada, *U.S. Geol. Surv. Prof. Pap.*, *466*, 62 pp.

Denny, C. S. (1967), Fans and pediments, *Am. J. Sci.*, *265*, 81–105.

Farr, T. G., and O. A. Chadwick (1996), Geomorphic processes and remote sensing signatures of alluvial fans in the Kun Lun Mountains, China, *J. Geophys. Res.*, *101*, 23,091–23,100.

Frankel, K. L., et al. (2007), Cosmogenic ^{10}Be and ^{36}Cl geochronology of offset alluvial fans along the northern Death Valley fault zone: Implications for transient strain in the eastern California shear zone, *J. Geophys. Res.*, doi:10.1029/2006JB004350, in press.

Gilbert, G. K. (1877), Geology of the Henry Mountains (Utah), in *U.S. Geographical and Geological Survey of the Rocky Mountain Region*, pp. 93–144, U.S. Gov. Printing Off., Washington, D. C.

Glenn, N. F., D. R. Streuker, D. J. Chadwick, G. D. Thackray, and S. J. Dorsch (2006), Analysis of LiDAR-derived topographic information for characterizing and differentiating landslide morphology and activity, *Geomorphology*, *73*, 131–148.

Haff, P. K. (2001), Desert pavement: An environmental canary?, *J. Geol.*, *109*, 661–668.

Haff, P. K. (2005), Response of desert pavement to seismic shaking, Hector Mine earthquake, California, 1999, *J. Geophys. Res.*, *110*, F02006, doi:10.1029/2003JF000054.

Haff, P. K., and B. T. Werner (1996), Dynamical processes on desert pavements and the healing of surficial disturbances, *Quat. Res.*, *45*, 38–46.

Hamilton, W. (1988), Detachment faulting in the Death Valley region, California and Nevada, *U.S. Geol. Surv. Bull.*, *1790*, 763–771.

Harvey, A. M., and S. G. Wells (2003), Late Quaternary variations in alluvial fan sedimentologic and geomorphic processes, Soda Lake basin, eastern Mojave Desert, California, *Spec. Pap. Geol. Soc. Am.*, *368*, 207–230.

Haugerud, R. A., D. J. Harding, S. Y. Johnson, J. L. Harless, C. S. Weaver, and B. L. Sherrod (2003), High-resolution lidar topography of the Puget Lowland, Washington, *GSA Today*, *13*, 4–10.

Horn, B. K. P. (1981), Hill shading and the reflectance map, *Proc. IEEE*, *69*, 14–47.

Hunt, C. B., and D. R. Mabey (1966), Stratigraphy and structure, Death Valley, California, *U.S. Geol. Surv. Prof. Pap.*, *494*, 137 pp.

Klinger, R. E. (2001), Stop A3: Evidence for large dextral offset near Red Wall Canyon, *U.S. Geol. Surv. Open File Rep.*, *01-51*, A32–A37.

Klinger, R. E. (2002), Quaternary stratigraphy and geomorphology of northern Death Valley—Implications for tectonic activity along the northern Death Valley fault, Ph.D. dissertation, 312 pp., Univ. of Colo., Boulder.

Knott, J. R., J. C. Tinsley III, and S. G. Wells (2002), Are the benches at Mormon Point, Death Valley, California, USA, scarps or shorelines?, *Quat. Res.*, *58*, 352–360.

Krabill, W. B., R. H. Thomas, C. F. Martin, R. N. Swift, and E. B. Frederick (1995), Accuracy of airborne laser altimetry over the Greenland ice sheet, *Int. J. Remote Sens.*, *16*, 1211–1222.

Li, J., T. K. Lowenstein, C. B. Brown, T. L. Ku, and S. Luo (1996), A 100 ka record of water tables and paleoclimates from salt cores, Death Valley, California, *Palaeogeogr. Palaeoclimatol. Palaeoecol.*, *123*, 179–203.

Lowenstein, T. K., J. Li, C. B. Brown, S. M. Roberts, T. L. Ku, S. Luo, and W. Yang (1999), 200 k.y. paleoclimate record from Death Valley salt core, *Geology*, *27*, 3–6.

Lubetkin, L., and M. M. Clark (1988), Late Quaternary activity along the Lone Pine fault, eastern California, *Geol. Soc. Am. Bull.*, *79*, 509–512.

Matmon, A., D. P. Schwartz, R. Finkel, S. Clemmens, and T. Hanks (2005), Dating offset fans along the Mojave section of the San Andreas fault using cosmogenic ^{26}Al and ^{10}Be, *Geol. Soc. Am. Bull.*, *117*, 795–807, doi:10.1130/B25590.1.

Matmon, A., K. Nichols, and R. Finkel (2006), Isotopic insights into smoothening of abandoned fan surfaces, southern California, *Quat. Res.*, *66*, 109–118.

McFadden, L. D., S. G. Wells, and M. J. Jercinovich (1987), Influences of eolian and pedogenic processes on the origin and evolution of desert pavements, *Geology*, *15*, 504–508.

McKean, J., and J. Roering (2004), Objective landslide detection and surface morphology mapping using high-resolution airborne laser altimetry, *Geomorphology*, *57*, 331–351.

Moring, B. (1986), Reconnaissance surficial geologic map of northern Death Valley, California and Nevada, scale 1:62,500, *U.S. Geol. Surv. Misc. Field Stud. Map*, *MF-1770*.

Nichols, K. K., P. R. Bierman, R. L. Hooke, E. M. Clapp, and M. Caffee (2002), Quantifying sediment transport on desert piedmonts using ^{10}Be and ^{26}Al, *Geomorphology*, *45*, 105–125.

Nichols, K. K., P. R. Bierman, M. C. Eppes, M. Caffee, R. Finkel, and J. Larsen (2005), Late Quaternary history of the Chemehuevi Mountain piedmont, Mojave Desert, deciphered using ^{10}Be and ^{26}Al, *Am. J. Sci.*, *305*, 345–368.

Nichols, K. K., P. R. Bierman, W. R. Foniri, A. R. Gillespie, M. Caffee, and R. Finkel (2006), Dates and rates of arid region geomorphic processes, *GSA Today*, *16*, 4–11.

Poage, M. A., and C. P. Chamberlain (2002), Stable isotopic evidence for a Pre-Middle Miocene rain shadow in the western Basin and Range: Implications for the paleotopography of the Sierra Nevada, *Tectonics*, *21*(4), 1034, doi:10.1029/2001TC001303.

Ritter, J. B., et al. (1993), Quaternary evolution of Cedar Creek alluvial fan, Montana, *Geomorphology*, *8*, 287–304.

Roering, J. J., J. W. Kirchner, and W. E. Dietrich (1999), Evidence for nonlinear, diffusive transport on hillslopes and implications for landscape morphology, *Water Resour. Res.*, *35*, 853–870.

Sartori, M. (2005), ALSM acquisition in Death Valley National Park, report on data processing, 13 pp., Natl. Cent. for Airborne Laser Mapping, Univ. of Fla., Gainesville.

Shrestha, R. L., W. E. Carter, M. Lee, P. Finer, and M. Sartori (1999), Airborne laser swath mapping: Accuracy assessment for surveying and mapping, *J. Am. Congr. Survey. Mapp.*, *59*, 83–94.

Staley, D. M., T. A. Wasklewicz, and J. S. Blaszczynski (2006), Surficial patterns of debris flow deposition on alluvial fans in Death Valley, CA using airborne laser swath mapping, *Geomorphology*, *74*, 152–163.

Taylor, J. R. (1997), *An Introduction to Error Analysis: The Study of Uncertainties in Physical Measurements*, 327 pp., Univ. Sci. Books, Sausalito, Calif.

Wallace, R. E. (1977), Profiles and ages of young fault scarps, north-central Nevada, *Geol. Soc. Am. Bull.*, *88*, 1267–1281.

Wells, S. G., L. D. McFadden, and J. C. Dohrenwend (1987), Influence of late Quaternary climatic changes on a desert piedmont, eastern Mojave desert, California, *Quat. Res.*, *27*, 130–146.

Wernicke, B., G. J. Axen, and J. K. Snow (1988), Basin and Range extensional tectonics at the latitude of Las Vegas, Nevada, *Geol. Soc. Am. Bull.*, *100*, 1738–1757.

Whipple, K. X., and T. Dunne (1992), The influence of debris-flow rheology on fan morphology, Owens Valley, California, *Geol. Soc. Am. Bull.*, *104*, 887–900.

J. F. Dolan and K. L. Frankel, Department of Earth Sciences, University of Southern California, Los Angeles, CA 90089, USA. (dolan@usc.edu; kfrankel@usc.edu)